Supplementary information

Multistep Nucleation Visualized During Solid-state Crystallization

Zhouyang Zhang,[a] Yujie Tang,[b] Yiran Ying,[c] Junqing Guo,[a] Min Gan,[a] Yateng Jiang,[a] Chunxian Xing,[a,b] Shanshan Pan,[b] Ming Xu,[c] Yangbo Zhou,[a] Haitao Zhang,[b*] Chi Wah Leung,[c] Haitao Huang,[c] Chee Leung Mak,[c*] and Linfeng Fei[a*]

[a] School of Physics and Materials Science, Jiangxi Key Laboratory for Two-Dimensional Materials, Jiangxi Engineering Laboratory for Advanced Functional Thin Films and Jiangxi Key Laboratory for Multiscale Interdisciplinary Study, Nanchang University, Nanchang, Jiangxi 330031, China

[b] Beijing Key Laboratory of Ionic Liquids Clean Process, Institute of Process Engineering, Chinese Academy of Sciences, Beijing 100190, China

[c] Department of Applied Physics, The Hong Kong Polytechnic University, Hung Hom, Kowloon, Hong Kong, China

E-mail: feilinfeng@gmail.com (L.F.); apaclmak@polyu.edu.hk (C.L.M.); htzhang@ipe.ac.cn (H.Z.)

This file includes:

Note S1
Figure S1 to Figure S16

Other Supplementary Materials for this manuscript include the following:

Movie S1 shows spinodal decomposition of the amorphous NiO nanosheet, suggesting the formation and evolution of spinodal structures under continuous electron-beam irradiation.

Movie S2 shows Oscillations between crystalline and amorphous state of NiO nuclei. The high-resolution TEM movie denmonstrates the nuclei underwent

reversible transitions between two states, which then resulted in the reconstruction of crystallographic orientation.

Supplementary Note S1

We have performed additional control experiments to confirm whether the oscillational behavior is induced by the irradiation of electron beam. Pre-synthesized sub-5 nm NiO nanoparticles were taken to the irradiation of electron beam within our TEM at a dose rate of 3825 electrons·$Å^{-2}$·s^{-1}. As shown in **Figure S16**, the left panel of **Figure S16a** shows 4 representative nanoparticles (nanoparticles # 1-3 were initially crystalline in structure while #4 was amorphous), which were continuously monitored for ~ 8 min. **Figure S16b** displays the whole monitoring process by 35 separated snapshots, and the result is schemed in the right panel of **Figure S16a**. The results simply show that all the nanoparticles (both crystalline and amorphous) maintained their structural states in the observed period (namely, no oscillation happened), which confirmed that the as-observed "oscillations" between amorphous and crystalline NiO nanoclusters in our study must not be induced by the irradiation of electron beam.

Generally, the electron beam damage to TEM specimens takes one of three principal forms, radiolysis (inelastic scattering, mainly electron-electron interactions such as ionization, breaks the chemical bonds of certain materials.), knock-on damage or sputtering (atoms displaced from the crystal lattice or ejected from the specimen surface), and heating (phonons heat specimen, especially for polymers and biological tissue) (*Transmission Electron Microscopy: A Textbook for Materials Science. Plenum Press, 1996.*). In this context, the thermal conductivity of NiO is 70-90 W/mK (*Journal of Physics C Solid State Physics 2001, 6, 2525*), so the heating effect is negligible in our case. Knock-on damage is directly related to the incident beam energy. For Ni, the maximum transferable kinetic energy at 200 keV, displacement energy and sputtering energy are 8.94, 22, 6-11 eV, respectively. So, the NiO nanocrystal may be damaged by sputtering near the surface rather than displacement of interior atoms, which also make negligible contribution for the dynamic and reversible transformations from the energy aspect. Therefore, the only effect of electron beam in our e-beam induced crystallization process is radiolysis (which promotes the decomposition of $Ni(OH)_2$ to NiO monomers, and then crystal nucleation originates mostly from thermal energy

depending on their diffusion). In short, the observed nucleation process is not an artifact of the e-beam irradiation.

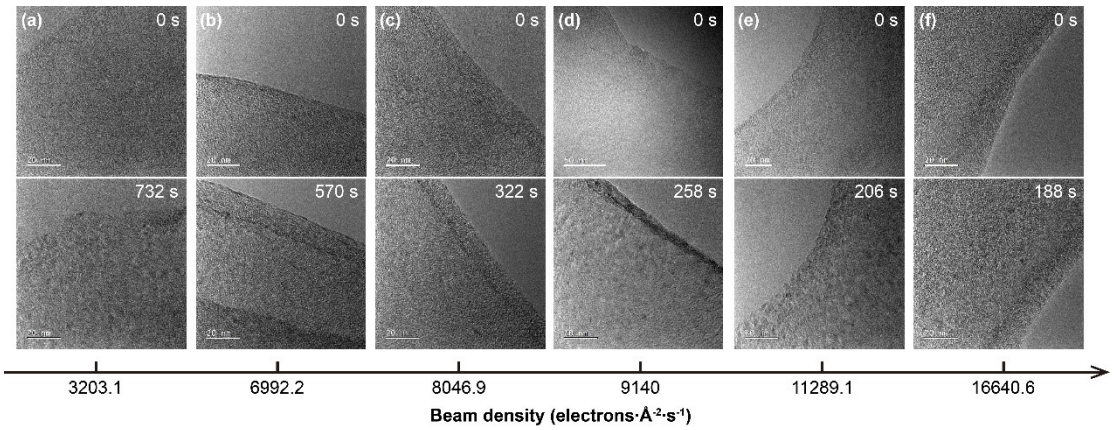

Figure S1. Influence of the electron-beam density on nucleation time. TEM images for NiO nucleation on 2D $Ni(OH)_2$ nanosheets induced by electron-beam irradiation at different densities. The beam density for (a), (b), (c), (d), (e) and (f) is 3203.1, 6992.2, 8046.9, 9140, 11289.1 and 16640.6 electrons·$Å^{-2}$·s^{-1}, respectively. The nucleation time is determined from the beginning of irradiation until an average nuclei diameter of ~3 nm. The corresponding beam-density-dependent nucleation time is shown in **Figure 1h**.

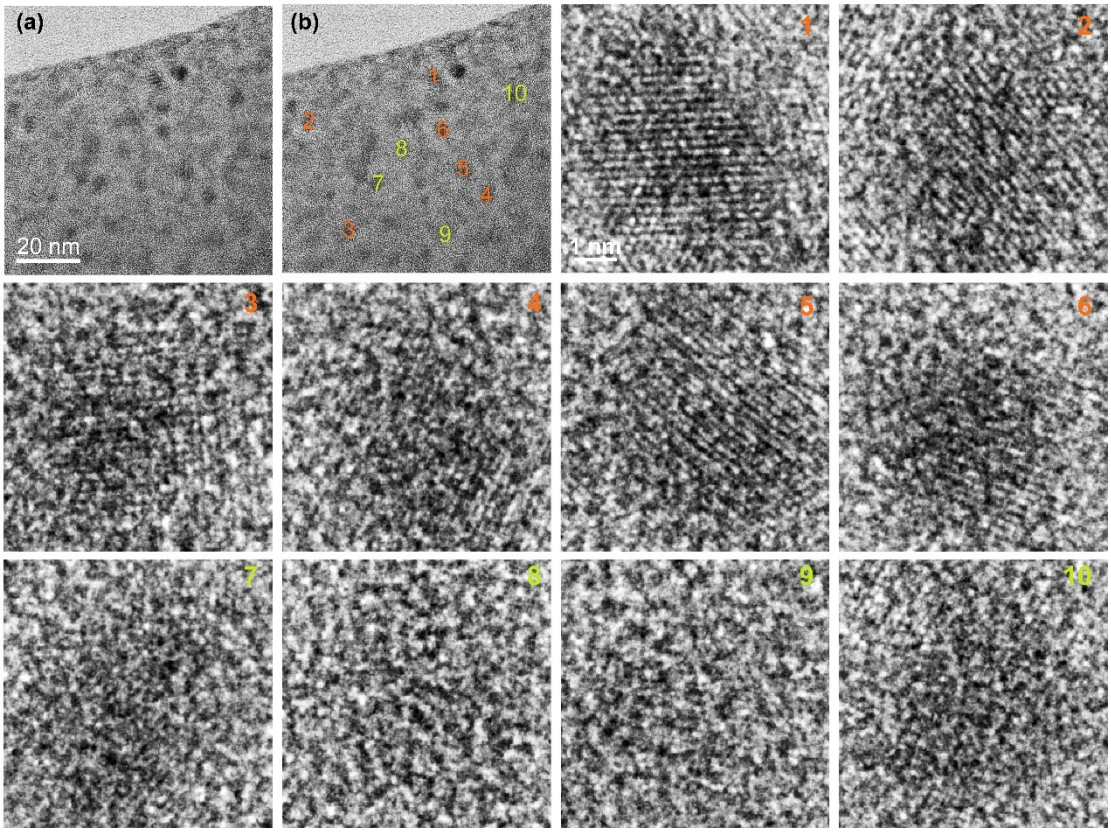

Figure S2. (a) The low-magnification bright-field TEM image containing multiple crystalline and amorphous clusters. (b) The zoom-in images for representative clusters in (a), showing their crystalline/amorphous natures. Scale bar in (a) also applies to the first panel of (b). Scale bar for cluster 1 also applies to other 9 clusters.

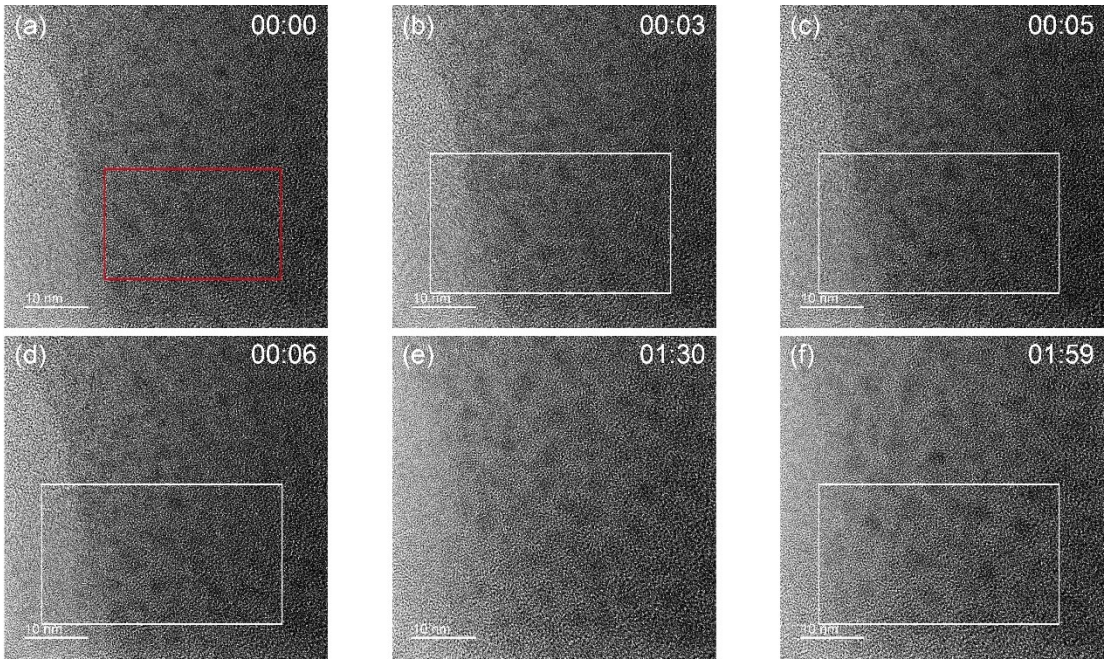

Figure S3. Spinodal decomposition of the amorphous nanosheet. (a-f) Sequential TEM images show the evolution of nanosheets into worm-like spinodal structures (Ni-rich and Ni-poor areas) and finally spherical nuclei. The regions delimited by white rectangles are sequentially captured as **Figure 3 a-d** in the main text. The zoom-in images for the region highlighted by red rectangle are shown in **Figure S4**.

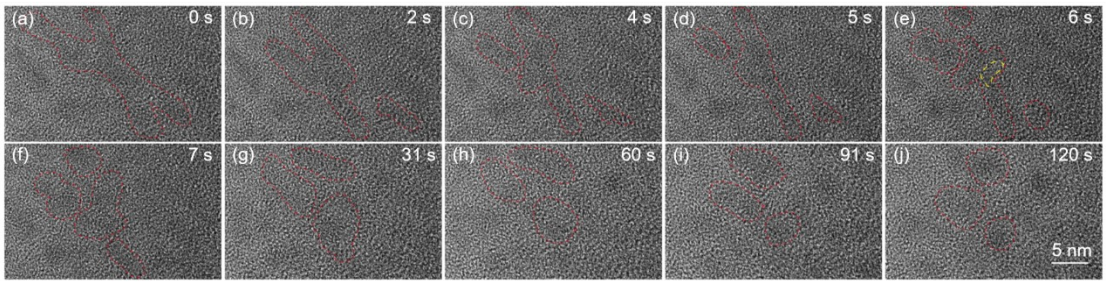

Figure S4. High-resolution images on spinodal decomposition of the amorphous nanosheet. In situ TEM image series for the evolution of Ni-rich regions during spinodal decomposition of the amorphous nanosheet. The region circled by yellow dashed line shows the unstable crystalline area.

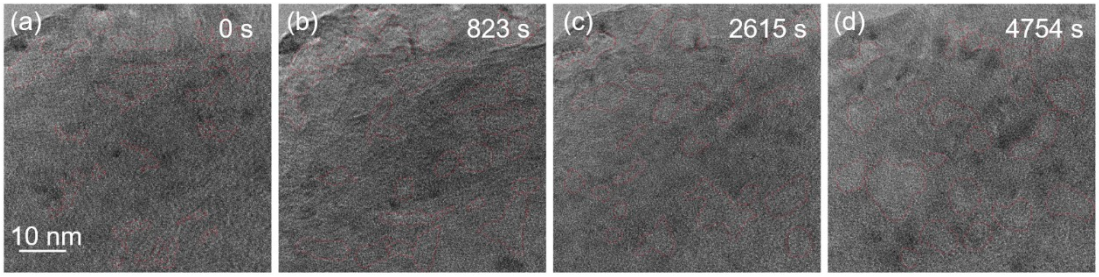

Figure S5. High-resolution images on spinodal decomposition of the amorphous nanosheet. In situ TEM image series for the evolution of Ni-poor regions during spinodal decomposition of the amorphous nanosheet.

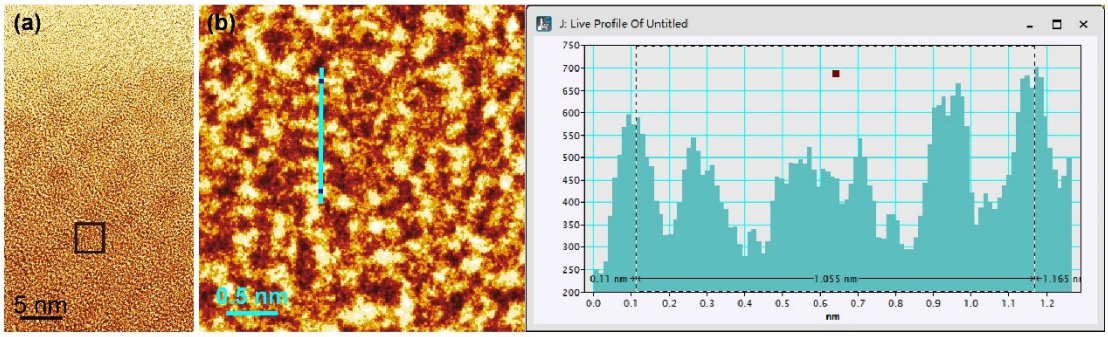

Figure S6. Characterization of nuclei in the spinodal structure. (a) TEM image for the spinodal structures (same as **Figure 3b** in the text). (b)Zoom-in image of the area denoted by black square in (a) showing the lattice fringes perpendicular to the cyan line. The interplane distances can be measured as 2.11 Å, which is consistent with NiO (200) of 2.0880 Å.

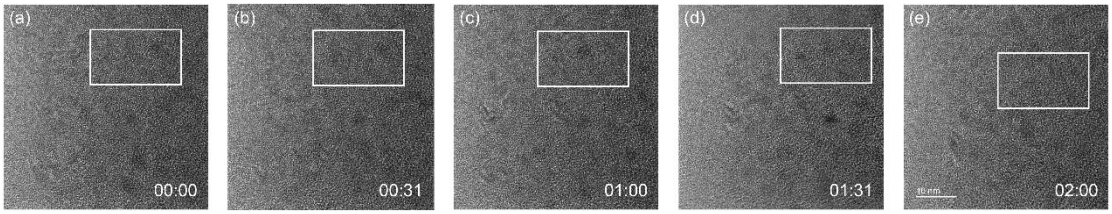

Figure S7. Long-range mass transport of a NiO cluster. (a-e) TEM sequences show the spherical NiO cluster in long-rang migration. The regions delimited by the white rectangles are sequentially captured as **Figure 3 f-j** in the main text.

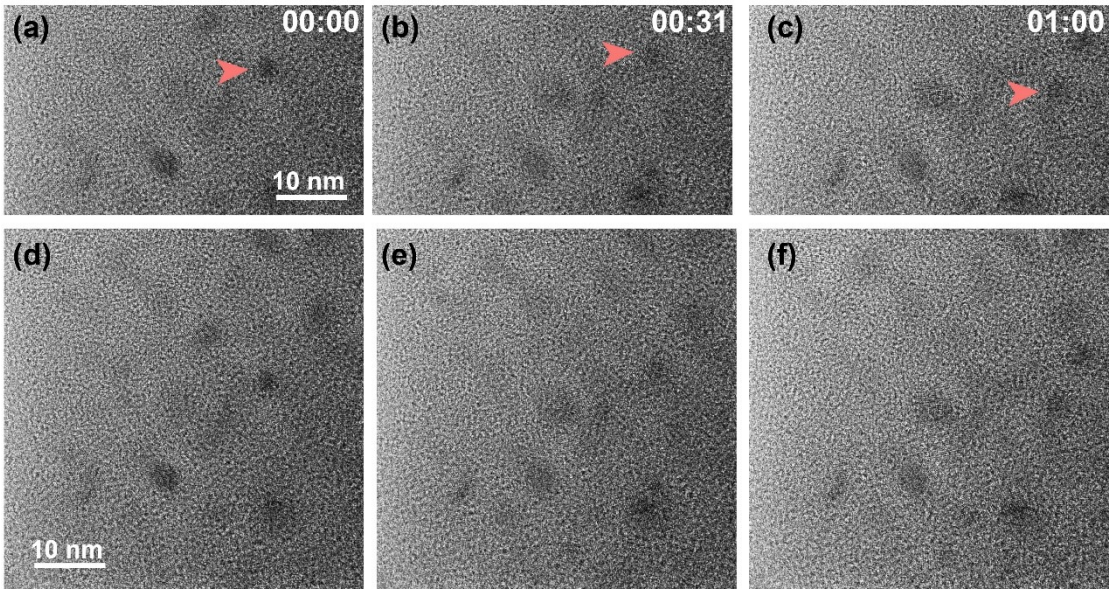

Figure S8. An additional example of mass transportation by a whole spherical cluster. (a-c) The TEM series shows the change of locations for a spherical cluster (indicated by red arrows) during mass transportation. (d-f) show the corresponding full resolution images.

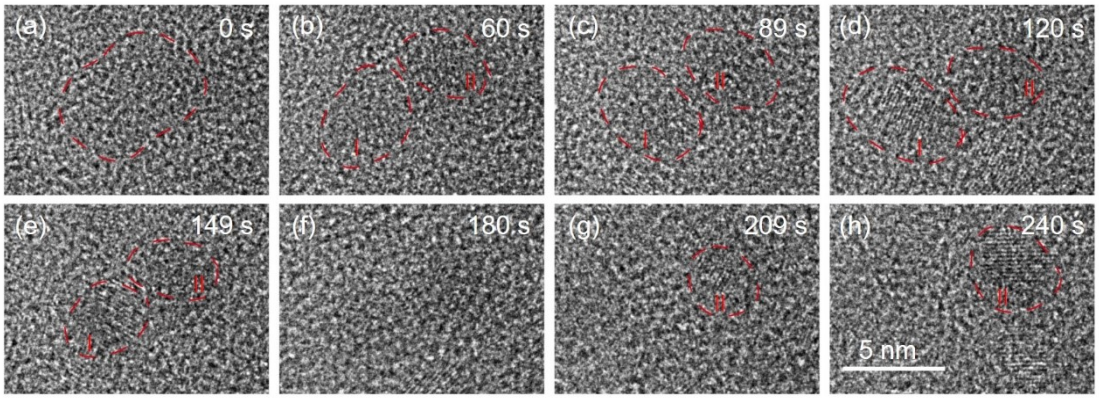

Figure S9. Examples of the crystallization-amorphization oscillations for NiO nuclei. (a-h) show the oscillation behavior between crystalline and amorphous states. Note that part of the nanocluster in (a) disassociated and dissolved in this process.

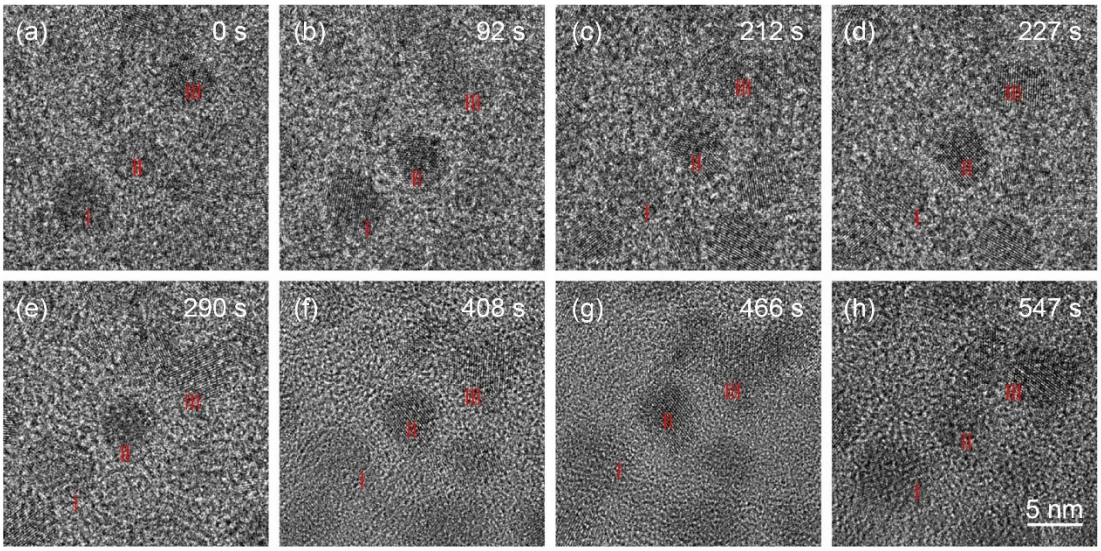

Figure S10. Examples of the crystallization-amorphization oscillations for NiO nuclei. (a-h) show the oscillation behavior between crystalline and amorphous states. The corresponding colored images with counterclockwise rotation of 90° are shown in **Figure 4a** in the main text.

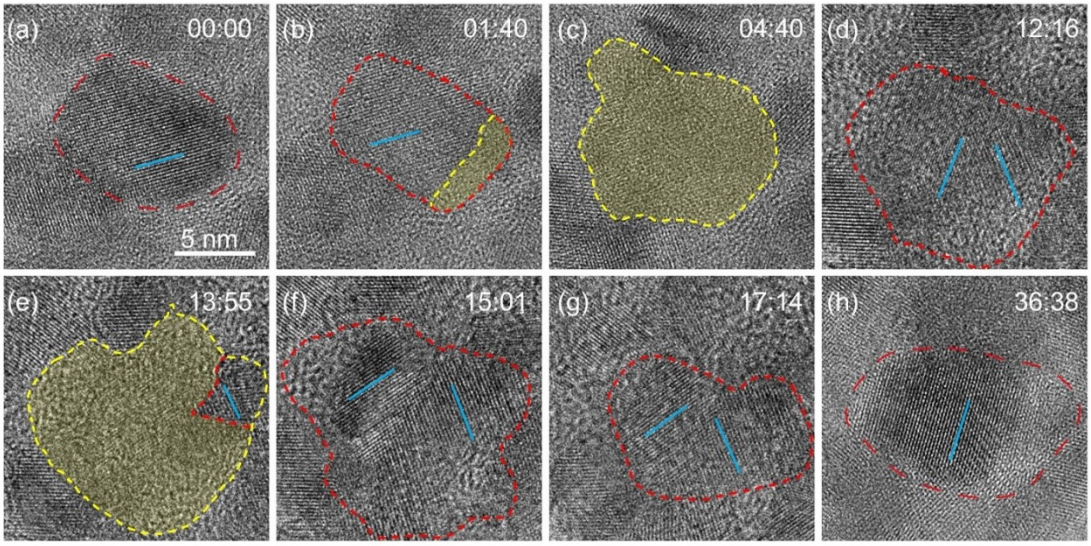

Figure S11. The amorphization-crystallization oscillations during a coalescing event. (a-h) TEM images show the merging of two neighboring nuclei with “oscillations”. The crystalline areas are circled by red dashed line. The amorphous areas are colored by yellow. The directions of lattice plane for the corresponding nuclei are indicated by blue lines.

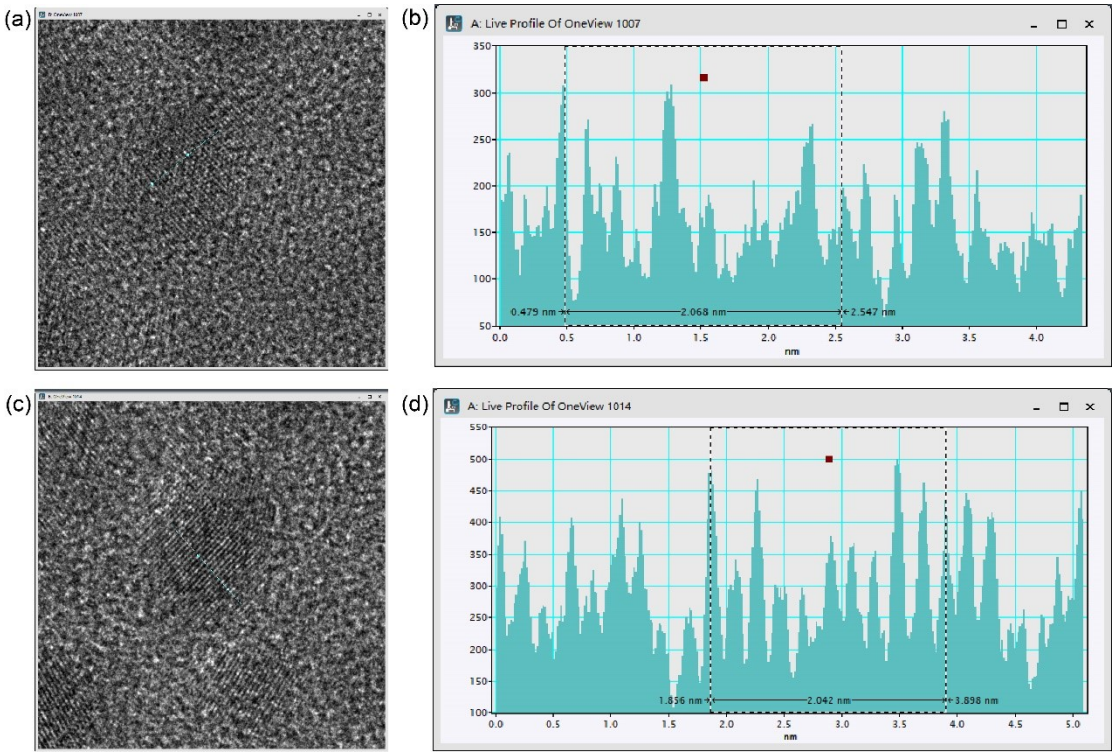

Figure S12. The measurements of interplane distances for the nuclei. The nascent nuclei in the first and final frames of **Figure 4b** are shown in (a) and (c), respectively. (b) and (d) measure the interplane distances of (a) and (c), with the results of 2.068 and 2.042 Å, respectively.

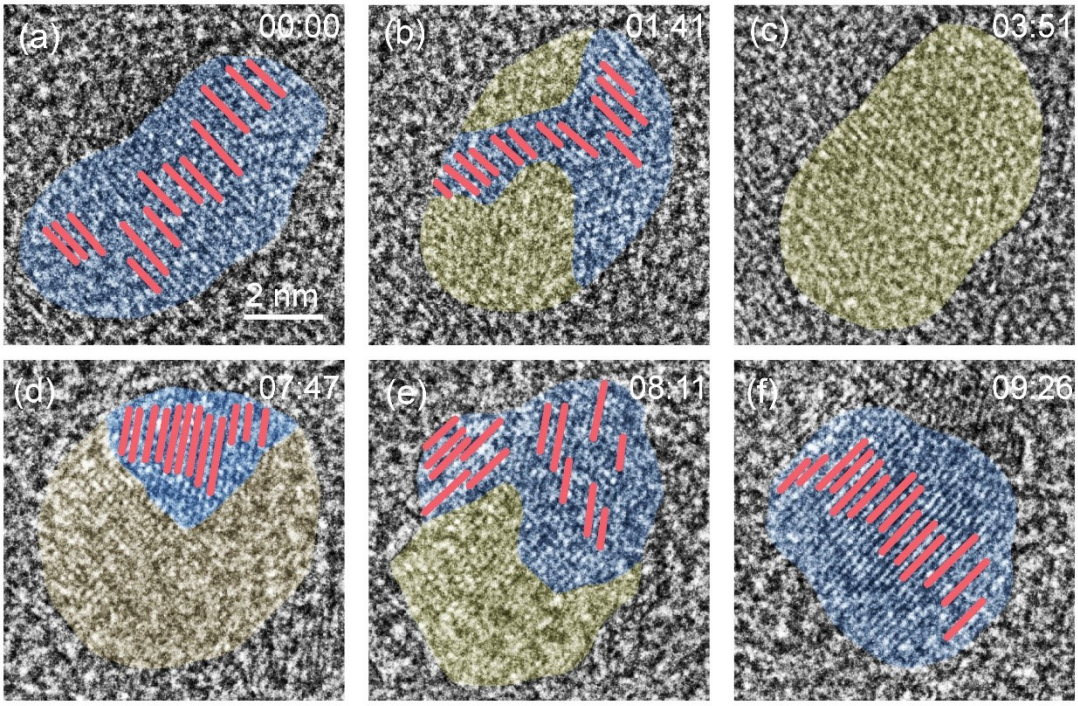

Figure S13. The measurement of the angles between (200) lattice plane and horizontal direction (left to right). The result is summarized in **Figure 4d** in the main text.

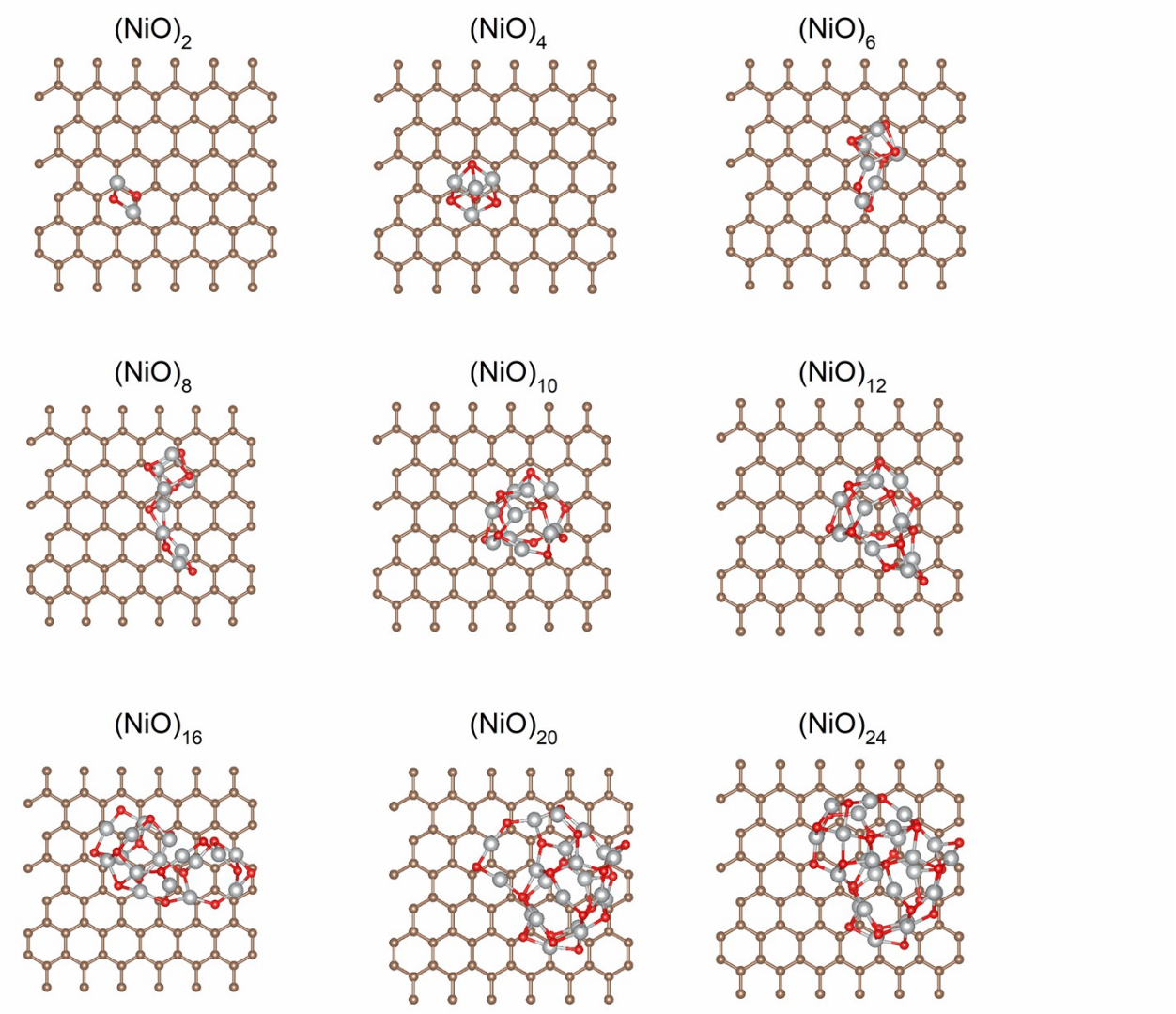

Figure S14. Structures of amorphous $(NiO)_n$ with different sizes on graphene substrate. C, Ni, and O atoms are represented in brown, grey, and red, respectively.

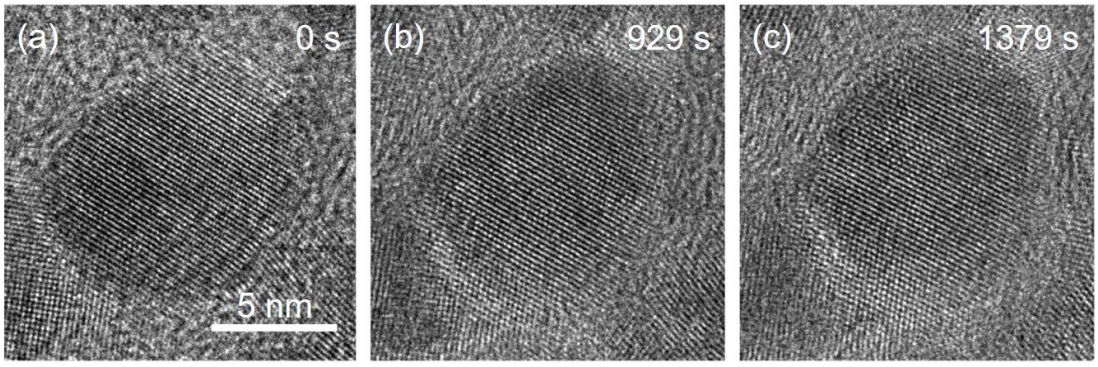

Figure S15. A large nanocrystal can maintain its crystalline nature during growth. (a)-(c) show that the crystallization-amorphization oscillations are hardly observed when the size of crystal increases.

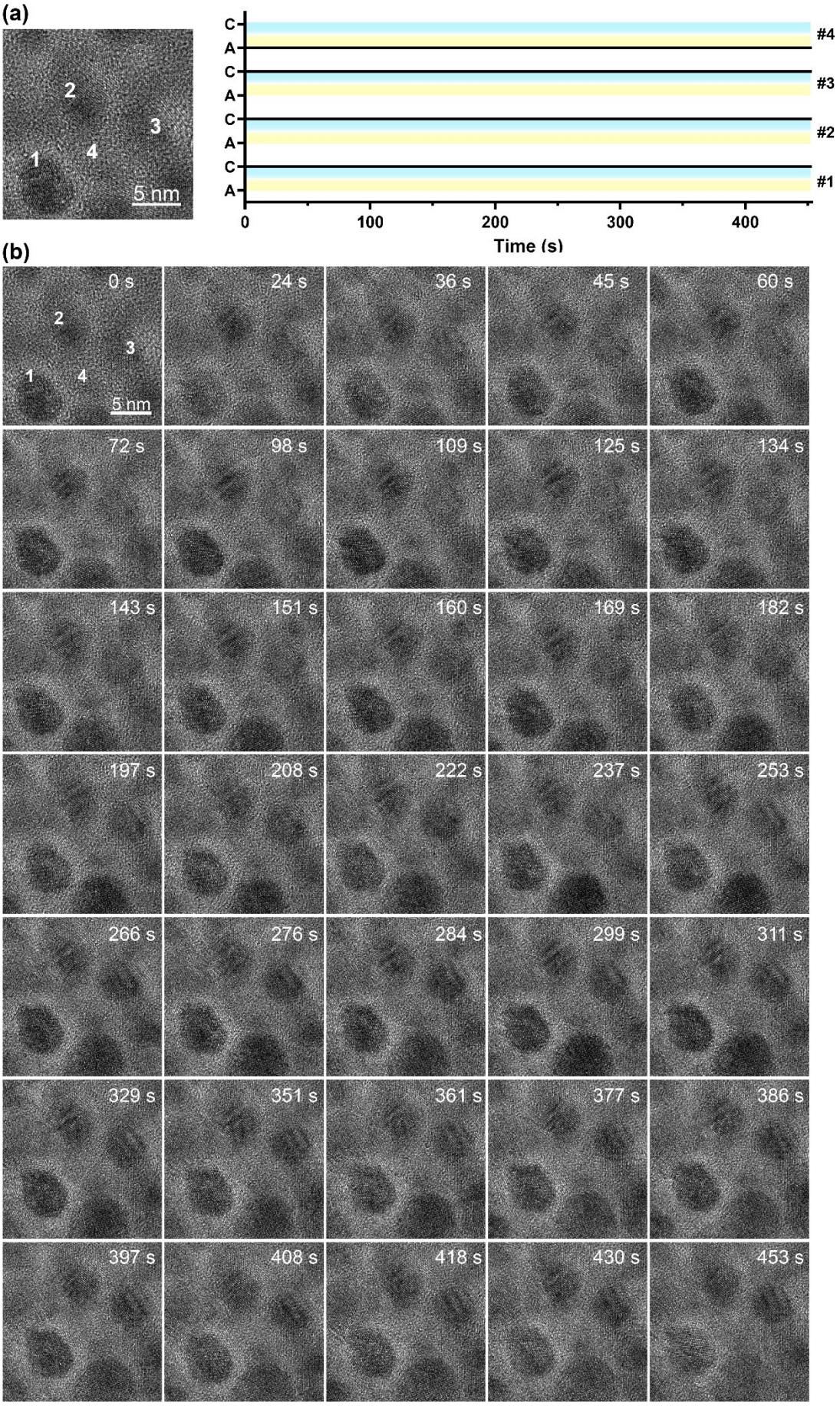
(a)
2
3
1
4
5 nm
C
A
C
A
C
A
C
A
#4
#3
#2
#1
0
100
200
300
400
Time (s)
(b)
0 s
24 s
36 s
45 s
60 s
2
3
1
4
5 nm
72 s
98 s
109 s
125 s
134 s
143 s
151 s
160 s
169 s
182 s
197 s
208 s
222 s
237 s
253 s
266 s
276 s
284 s
299 s
311 s
329 s
351 s
361 s
377 s
386 s
397 s
408 s
418 s
430 s
453 s

Figure S16. **Comparison experiment to rule out the effect of beam irradiation on oscillation.** (a)The trajectories of structural states for four pre-synthesized NiO nanoparticles under the continuous irradiation of electron beam. (b) The corresponding in situ TEM image series for this four NiO nanoparticles under the continuous irradiation of electron beam.